



Article

Xanthophylls Modulate Palmitoylation of Mammalian β -Carotene Oxygenase 2

Sheetal Uppal ¹, Sergey A. Dergunov ², Weiyu Zhang ², Susan Gentleman ¹, T. Michael Redmond ^{1,*}, Eugene Pinkhassik ^{2,*} and Eugenia Poliakov ^{1,*}

¹ Laboratory of Retinal Cell & Molecular Biology, National Eye Institute, National Institutes of Health, Bethesda, MD 20892, USA; sheetal.uppal2@nih.gov (S.U.); sbgman@verizon.net (S.G.)

² Department of Chemistry, University of Connecticut, Storrs, CT 06269, USA; sergey.dergunov@uconn.edu (S.A.D.); weiyu.zhang@uconn.edu (W.Z.)

* Correspondence: redmondd@nei.nih.gov (T.M.R.); eugene.pinkhassik@uconn.edu (E.P.); poliakove@nei.nih.gov (E.P.)

Abstract: An extensive body of work has documented the antioxidant role of xanthophylls (lutein and zeaxanthin) in human health and specifically how they provide photoprotection in human vision. More recently, evidence is emerging for the transcriptional regulation of antioxidant response by lutein/lutein cleavage products, similar to the role of β -carotene cleavage products in the modulation of retinoic acid receptors. Supplementation with xanthophylls also provides additional benefits for the prevention of age-related macular degeneration (AMD) and attenuation of Alzheimer’s disease symptoms. Mammalian β -carotene oxygenase 2 (BCO2) asymmetrically cleaves xanthophylls as well as β -carotene in vitro. We recently demonstrated that mouse BCO2 (mBCO2) is a functionally palmitoylated enzyme and that it loses palmitoylation when cells are treated with β -carotene. The mouse enzyme is the easiest model to study mammalian BCO2 because it has only one isoform, unlike human BCO2 with several major isoforms with various properties. Here, we used the same acyl-RAC methodology and confocal microscopy to elucidate palmitoylation and localization status of mBCO2 in the presence of xanthophylls. We created large unilamellar vesicle-based nanocarriers for the successful delivery of xanthophylls into cells. We demonstrate here that, upon treatment with low micromolar concentration of lutein (0.15 μ M), mBCO2 is depalmitoylated and shows partial nuclear localization (38.00 \pm 0.04%), while treatment with zeaxanthin (0.45 μ M) and violaxanthin (0.6 μ M) induces depalmitoylation and protein translocation from mitochondria to a lesser degree (20.00 \pm 0.01% and 35.00 \pm 0.02%, respectively). Such a difference in the behavior of mBCO2 toward various xanthophylls and its translocation into the nucleus in the presence of various xanthophylls suggests a possible mechanism for transport of lutein/lutein cleavage products to the nucleus to affect transcriptional regulation.

Citation: Uppal, S.; Dergunov, S.A.; Zhang, W.; Gentleman, S.; Redmond, T.M.; Pinkhassik, E.; Poliakov, E. Xanthophylls Modulate Palmitoylation of Mammalian β -Carotene Oxygenase 2. *Antioxidants* **2021**, *10*, 413. <https://doi.org/10.3390/antiox10030413>

Academic Editor: Torsten Bohn

Received: 30 January 2021

Accepted: 2 March 2021

Published: 9 March 2021

Publisher’s Note: MDPI stays neutral with regard to jurisdictional claims in published maps and institutional affiliations.



Copyright: © 2021 by the authors. Licensee MDPI, Basel, Switzerland. This article is an open access article distributed under the terms and conditions of the Creative Commons Attribution (CC BY) license (<http://creativecommons.org/licenses/by/4.0/>).

1. Introduction

Most consideration of the antioxidant function of xanthophylls, polar hydroxy carotenoids, has focused on their chemical role in quenching excited triplet states of singlet oxygen by virtue of their extended conjugated bond systems. However, there is emerging evidence for a role of xanthophyll/xanthophyll cleavage products in modulating transcriptional regulation of antioxidant gene pathways.

In respect of their best-known role, high dietary intake of xanthophylls may offer protection against age-related macular degeneration (AMD), cancer and neurodegenerative diseases [1,2]. While xanthophylls account for less than 20% of the total carotenoids in the human diet, in the blood plasma the amount of xanthophylls increases to about 40% and is increased even more in the brain and retina [3,4]. Thus,

xanthophylls account for about 70% of total carotenoids in all brain regions. Xanthophylls are selectively concentrated in the most vulnerable regions of polyunsaturated lipid-enriched membranes, such as in the retinal photoreceptor outer segments [5]. This localization is ideal for macular xanthophylls to act as lipid-soluble antioxidants, which is the most likely mechanism of protection against photooxidation [6]. Additionally, the high membrane solubility and preferential transmembrane orientation of macular xanthophylls [6,7] enhance their chemical and physical stability in retina and brain membranes [8] and maximize their protective action against oxidative stress in these organs [9]. Xanthophylls are capable of quenching excited triplet states of potent singlet oxygen photosensitizers. Free all-*trans*-retinal may absorb light and transfer energy from its excited triplet state to molecular oxygen, generating singlet oxygen [10]. It is postulated that the close proximity of xanthophylls allows effective energy transfer from excited all-*trans*-retinal to xanthophyll and prevents singlet oxygen generation by this photosensitizer [11]. By this mechanism, the largest part of excess energy can be transferred from potentially harmful triplets of photosensitizers to xanthophylls and dissipated as heat. The ratio of zeaxanthin (and *meso*-zeaxanthin) to lutein is higher in the macula where the strongest light is received compared to peripheral low-light-vision regions of the eye [3]. A portion of dietary lutein is converted to *meso*-zeaxanthin, a stereoisomer of zeaxanthin, presumably in retinal pigment epithelium (RPE) by RPE65 isomerase [12]. This preference for zeaxanthin has been suggested to be due to a greater antioxidant capacity, possibly due to the longer system of conjugated double bonds and membrane-stabilizing function of zeaxanthin (and *meso*-zeaxanthin) compared to lutein [12,13]. Xanthophylls are delivered to the retina with the help of high-density lipoprotein (HDL) [14] and xanthophyll-binding proteins [15]. Xanthophyll-binding proteins have been described for both zeaxanthin and lutein [16]. However, the role of β -carotene oxygenase 2 (BCO2), an enzyme that can cleave xanthophylls [17], is not thoroughly studied.

BCO2 is present in the brain, retina and RPE; everywhere xanthophylls accumulate. BCO2 is well characterized as a carotenoid metabolizing enzyme [18–21] that is widely distributed in tissues, including the retina, RPE, skeletal muscle, small intestine and liver [22]. A deficiency of BCO2 was found to be associated with accumulation of carotenoids in the adipose tissues [23], such as subcutaneous adipose tissue. This leads to the occurrence of yellow fat in sheep [24], cow [25], and yellow skin in chicken [26]. The abSNP rs2250417 in BCO2 has one of the strongest instances of statistical significance for association with AMD of carotenoid metabolism genes [27]. The two minor alleles for SNP rs2250417 in BCO2 account for an increase in risk for AMD by almost 50% [27]. Additionally, BCO2 deficiency in mice leads to stimulation of oxidative stress and inflammation in hypothalamic tissues on a low carotenoid diet [28].

To better study the role of BCO2 in metabolism of xanthophylls, we developed xanthophyll-containing large unilamellar vesicles (LUVs) to efficiently deliver xanthophylls to cells. We chose to express mBCO2 in human cell culture because it has only one major isoform while human and monkey BCO2 have several major isoforms. Only one of these has a N-terminal mitochondrial signal and it is still hotly debated if this isoform manifests as an active BCO2 enzyme [17,29–31]. Here, using LUVs, we describe that lutein modulates the palmitoylation status of mouse BCO2 (mBCO2) and changes its cellular localization in HEK293F cells from mitochondria to nucleus upon binding. We have detected the same effect for zeaxanthin and violaxanthin but to a lesser degree and our modeling analysis suggests a possible explanation of the difference. Accumulation in the nucleus of mBCO2 loaded with xanthophylls could directly affect gene expression and may provide a mechanism whereby xanthophylls/xanthophyll cleavage products could elicit a transcriptional response to oxidant stress.

2. Materials and Methods

2.1. Materials

1,2-dimyristoyl-sn-glycero-3-phosphocholine (DMPC), 1,2-dimyristoyl-sn-glycero-3-phospho-L-serine (sodium salt) (DMPS), 1,2-dipalmitoyl-sn-glycero-3-phosphocholine (DPPC), 1,2-dipalmitoyl-sn-glycero-3-phospho-L-serine (sodium salt) (DPPS) were purchased from Avanti Polar Lipids, Inc. (Alabaster, AL, USA). (R)-(+)-limonene and tricine were used as received (Sigma-Aldrich, St. Louis, MO, USA). Nitrogen-purged hexane, dichloromethane (DCM) and chloroform (CHCl_3) were passed through an activated alumina column, dried with CaSO_4 , and stored over 4 Å molecular sieves. All kinetic experiments were performed with the same batch of samples. Lutein and violaxanthin were purchased from Cayman Chemicals (Ann Arbor, MI, USA), and zeaxanthin (65%) from Toronto Research Chemicals (Toronto, ON, Canada).

2.2. Preparation of Large Unilamellar Vesicles (LUVs) with Xanthophylls

Aqueous lipid dispersions of LUVs were prepared by first mixing the required amounts of lipids, carotenoids, and limonene (used here for better solubilization of carotenoids in the lipid bilayer) in chloroform. All samples were prepared using similar protocol to the one described previously [32]. Amounts of lipids were the same, 10 mg/mL, limonene: lipid = 1:1 (mol/mol), while amounts of carotenoids were different: 0.5 mg zeaxanthin in 1.5 mL of buffer (using DPPC/DPPS or DMPC/DMPS lipids); the lutein preparation contained 0.25 mg lutein in 1.5 mL of buffer (using DMPC/DMPS lipids); and the violaxanthin preparation contained 0.25 mg violaxanthin in 1.5 mL of buffer (using DMPC/DMPS lipids). All samples were prepared with a mole fraction of 7% PS (sn-glycero-3-phospho-L-serine) to avoid multilamellar stack formation [33]. The solvent was evaporated with an inert gas stream to constant weight. The lipid film was hydrated with 100 mM tricine-KOH pH 8.0 buffer (prepared with H_2O) at room temperature with intermittent gentle vortex mixing. The lipid suspension was passed through 0.4, 0.2, 0.1 μm Nucleopore polycarbonate membranes (21 times through each membrane) using a mini-extruder (Avanti Polar Lipids). The LUVs were mixed with hexane and shaken gently for 20 min to remove limonene as confirmed by GC-MS. The LUVs were then decanted from the organic layer and the aqueous solution was purged with nitrogen and degassed to remove traces of hexane.

2.3. Generation of Expression Vectors

Mouse BCO2 cDNAs were prepared as described [34] and used to generate vectors for the expression of BCO2 in mammalian cells. Briefly, BCO2 was subcloned into the bicistronic expression vector pVitro2 (InvivoGen, San Diego, CA, USA) and into the Gateway cloning vector pcDNA6.2c-Lumio-DEST vector (Thermo Fisher (Invitrogen), Carlsbad, CA, USA) to generate untagged or C-terminal V5/lumio tagged versions of mouse BCO2, respectively. All constructs and mutants were sequenced to verify the orientation and accuracy of the ORFs and/or the changes introduced.

2.4. Cell Culture

Human 293F FreeStyle (Thermo Fisher, Invitrogen) suspension cells were grown in serum-free FreeStyle 293 expression medium (Invitrogen) and transfected according to the previously published protocol [35]. Briefly, a typical transfection experiment used 3×10^7 cells in 28 mL of FreeStyle medium mixed with 2 mL of OptiMem-I reduced serum medium containing 40 μL 293fectin transfection reagent (Invitrogen) and 20 μg of each expression plasmid under study. Cells were grown with shaking at 125 rpm on an orbital shaker platform in a 37 °C incubator with a humidified atmosphere of 8% CO_2 for 48 h total. In total, 200 μl of vesicles with xanthophylls were added, incubating for 5 hr under standard growth conditions.

2.5. Antibodies

Rabbit polyclonal antibody 186 was custom made against the mouse BCO2 multiple antigenic peptides (MAP)-SKFLQSDTYKANSAG peptide and 7055 rabbit polyclonal antibody was produced by co-immunization of the two human BCO2 MAP-SHENLHQEDLEKEGGIE and MAP-QDNGRTLEVYQLQNLRKAG peptides.

2.6. Characterization of Large Unilamellar Vesicles (LUVs) with Xanthophylls

2.6.1. Dynamic Light Scattering (DLS)

The hydrodynamic diameter and polydispersity index (PDI) were measured at 30 °C on a Malvern Nano-ZS zetasizer (Malvern Instruments Ltd., Worcestershire, UK) equipped with a 4 mW helium-neon laser operated at 633 nm with a fixed scattering angle of 173°. An 80 µL sample was placed into disposable cuvettes without dilution (70 µL, center height 8.5 mm, BRAND® UV-Cuvette micro). Data were processed using non-negative least squares (NNLS) analysis.

2.6.2. GC-MS Analysis

A Shimadzu GC-2010 Plus system with an AOC-20i Auto-Injector and a GCMS-QP2010 SE ion trap MS system (Shimadzu, Kyoto, Japan) was used for GC-MS analysis using the electron impact ionization mode. Chromatographic separations were performed on a Shimadzu SH-Rxi-5SiL MS capillary column (30 m × 0.25 mm, 0.25 mm film thickness; non-polar phase: Crossbond™ 100% dimethyl polysiloxane as stationary phase). The temperatures of the injector and the GC-MS transfer line were 170 and 280 °C, respectively. The carrier gas was ultrahigh purity helium (Airgas); the flow rate was 1.0 mL/min. The mass spectrometer was operated using the following parameters: the ratio of the split injection was 20:1, ionization voltage was 70 eV; ion source temperature was 200 °C; scan mode, 30.0–500.0 (mass range); scan rate, 5000 amu/s, and 3.68 scans/s; start time was 2 min. Electron multiplier (EM) voltage was obtained from autotune. The oven temperature was programmed to hold at 60 °C for 2 min, increase to 300 °C at 50 °C/min, and hold at 300 °C for 3 min.

To measure the residual limonene in LUVs, a 100 µL aliquot is mixed with 1.9 mL of hexane and 50 mg of CaSO₄ (used here to disrupt the LUVs) and stirred for 30 min to extract limonene. The data were averaged from at least three independent measurements.

2.6.3. Small-Angle X-Ray Scattering (SAXS)

The structural characteristics of LUVs were studied using small-angle X-ray scattering (SAXS). SAXS patterns were obtained using a Bruker NanoStar instrument equipped with a turbo rotating anode operated at 50 kV and 50 mA, evacuated beam path, two-pinhole collimators, Göbel mirrors selecting Cu-K α radiation, and a large 2D Vantec-2000 detector. Samples were measured in 1.5 mm quartz capillaries; the measurement time was 3 h. Scattering patterns were collected in the range $0.006 \text{ \AA}^{-1} < q < 0.35 \text{ \AA}^{-1}$. The sample to detector distance of 67.8 cm was verified using silver behenate as a calibration standard. The SAXS patterns were corrected for sample transmission and empty cell scattering. One-dimensional (1D) SAXS patterns were obtained by azimuthal integration of the resulting 2D images around the beam center, to obtain the intensity (ISAXS) vs. q profiles. The magnitude of the scattering vector was calculated as $q = (4\pi/\lambda) \sin(\theta/2)$, where θ is the scattering angle and λ is the X-ray wavelength for Cu-K α ($\lambda = 1.5418 \text{ \AA}$).

2.6.4. Spectroscopic Determination of the Concentration of Xanthophylls

The concentrations of xanthophylls were measured using a 2 mm optical path quartz cell in an Agilent Cary 60 UV-Vis spectrophotometer. To measure the concentration of xanthophylls in LUVs, a 10 µL aliquot is mixed with 300 µL of DMF. Standards and samples were measured at least 3 times and the data were averaged. Final concentrations of xanthophylls in LUVs measured by UV/Vis: zeaxanthin 0.038 g/L (DPPC/DPPS,

0.45 μ M final), zeaxanthin 0.14 g/L (DMPC/DMPS); lutein 0.0125 g/L (DMPC/DMPS, 0.15 μ M and 0.06 μ M final); violaxanthin 0.07 g/L (DMPC/DMPS, 0.6 μ M final).

2.7. BCO2 Protein Palmitoylation Was Analyzed by Acyl-Resin-Assisted Capture (Acyl-RAC)

For cell lysis and the Acyl-RAC assay, we followed the same protocol as previously described in detail, with slight modifications [34,36]. BCO2-overexpressing HEK293F cells were washed with 1X-PBS and resuspended in lysis buffer (50 mM HEPES (pH 7.4) containing 150 mM NaCl, 5 mM EDTA, 1% glycerol, and 1X complete protease inhibitor cocktail (Roche Diagnostics)). Resuspended cells were lysed using N₂ cavitation followed by centrifugation at 900 \times g for 10 min at 4 °C to remove the cell debris and nuclei. The clarified supernatant was then subjected to centrifugation at 20,000 \times g for 30 min at 4 °C to obtain heavy membrane (mitochondrial) pellet and post-mitochondrial supernatant (light membrane and cytosol) fractions. Typically, a 1000 μ g amount of resuspended heavy membrane pellet protein (resuspended in lysis buffer containing 0.1% Triton X-100) was used for palmitoylation detection assay. Briefly, free cysteine sulphydryl (-SH) groups were blocked with 0.5% (v/v) S-methyl methanethiosulfonate (MMTS) containing blocking buffer for 15 min at 40 °C. The blocked protein samples were then subjected to acetone protein precipitation. The protein pellet was then resuspended in 550 μ L 100 mM HEPES containing 5 mM EDTA and 1% SDS (v/v). The samples were then divided into two 250 μ L aliquots (containing 400 μ g protein amount) and the remaining 50 μ L was used as an input. The samples were treated with 250 mM hydroxylamine (NH₂OH, HAM) or control (250 mM NaCl). To capture proteins with free -SH groups, each sample was mixed with 10 mg activated thiol-sepharose 4B beads (Sigma) and incubated for 2 h at room temperature with continuous end-over-end rotation. After incubation, the beads were washed, and bound proteins were eluted by boiling the beads with an aliquot of 50 μ L elution sample buffer. The input and eluted fractions from “HAM” and “control” samples were separated by SDS-PAGE and analyzed by Western blotting.

2.8. Immunocolocalization Studies BCO2 Protein in Different Organelles upon Substrate Treatment Using Confocal Microscopy

BCO2-overexpressing COS7 cells (1 \times 10⁶ cells/mL) seeded on poly L-lysine coated 18 mm coverslips were analyzed by immunofluorescence microscopy to determine the localization of BCO2 protein in different subcellular organelles as described previously [34]. Briefly, COS7 cells were transfected with 20 μ g of BCO2-Lumio V5 tag plasmid using Fugene® 6 transfection reagent (1:6 DNA: Fugene 6 ratio). After 43 h, BCO2-transfected cells were treated with substrate-encapsulated LUVs for 5 h. Fixed cells were immunostained with V5 monoclonal and polyclonal antibodies alone and together with primary antibodies specific for different subcellular organelles (ER (PDIA3), Golgi (MAN2A1), mitochondria (COX IV and HSP60), and peroxisomes (PMP70)), followed by Alexa fluorophore-conjugated secondary antibodies (Invitrogen). Cell nuclei were stained with DAPI (1 μ g/ μ L solution; Sigma). Slides were then visualized with a Zeiss LSM 700 confocal microscope using a 40X oil immersion lens/1.4-NA and Zeiss ZEN software. Pearson’s correlation coefficient values were determined for analysis of the co-localization of BCO2 protein and different organelles and represented as mean \pm standard deviation. For nuclear co-localization of BCO2 protein, we measured the Pearson’s correlation coefficient of BCO2 with DAPI-stained nuclei using the results from three independent experiments: single labeling of BCO2 “alone”, double labeling of BCO2 with mitochondrial markers COX IV and HSP60. Results shown were typical of a minimum of three independent experiments with 5–10 fields of view containing on average 1–10 cells/field of view. For quantification and statistical analyses, at least 100 cells were observed for each organelle and nuclear co-localization.

2.9. Construction of Models and Ligand Docking Simulations

A model of mBCO2 was constructed with the Swiss-Model program using the RPE65 4F30 crystal as a template [37]. The loop carrying the PDPCCK motif is unresolved in this crystal and is given in this model as a random loop. To model the unresolved areas, the mBCO2 sequence with distances specified for the catalytic histidines was submitted to the I-Tasser server [38–40]. Five models were obtained; however, the side chains of the Fe-coordinating histidines and glutamates were displaced relative to both the Swiss-Model and RPE65 crystals. The sidechains of the histidines and glutamates of the top I-Tasser model were modified based on the Swiss-Model and the RPE65 crystal structures. Finally, to model an active state, the Fe center and the O₂ and OH of the VP14 crystal (PDB: NPE3) were aligned with both models and integrated into the models. Clashes resulting from the introduction of O₂ and OH on the Fe center were corrected by torsioning the relevant residues. Ligand dockings were carried out using Autodock Vina [41]. In general ligand restraints chosen allowed for all possible torsions.

3. Results

3.1. Xanthophyll Delivery System

LUVs were prepared by hydration of lipid with carotenoids and assisting limonene, followed by extrusion and extraction of limonene to yield unilamellar vesicles with a narrow size distribution, as confirmed by SAXS and DLS, respectively (Figure 1). The amount of carotenoids associated with LUVs was determined by UV-vis spectroscopy following a previously published protocol [42]. Previously, it was shown that, depending on the structure of the substrate, as well as on the composition of lipids, hydrophobic carotenoids are oriented differently in the phospholipid bilayer of delivery vesicles [43]. Thus, symmetrically oxy-functionalized carotenoids intercalate into phospholipid membranes perpendicular to the membrane surface [44], while fully non-polar β-carotene is intercalated parallel to the surface within the hydrophobic core of phospholipid bilayers [44,45]. In addition, the molecular length of a carotenoid affects the degree of its intercalation into phospholipid bilayers, depending on the membrane thickness [42]. In fact, zeaxanthin (C₄₀) was better incorporated into unilamellar vesicles of dimyristoylphosphatidylcholine (n-C₁₄), whereas decaprenozeaxanthin (C₅₀) was better adopted in unilamellar vesicles of dipalmitoylphosphatidylcholine (n-C₁₆). On the other hand, the inclusion of large hydrophobic molecules into the phospholipid bilayer can change the structure as well as the thickness of vesicles [46]. To understand the membrane structure of vesicles as well as the organization of carotenoids within DMPC and DPPC LUVs with associated zeaxanthin, X-ray scattering measurements were performed. The phosphate-phosphate (p-p) thicknesses obtained from the SAXS data fit gave values of ~35.1 Å for DMPC-zeaxanthin membranes and ~41.2 Å for DPPC-zeaxanthin membranes, which is the typical thickness for DMPC and DPPC-carotenoid LUVs [42,46]. The length values (Figure 1) of the carotenoid (lutein or zeaxanthin) correspond well to the length of the lipophilic segment of DMPC, but not DPPC. This is the reason for the much weaker incorporation of lutein (or zeaxanthin) into DPPC membranes compared to DMPC [42,47].

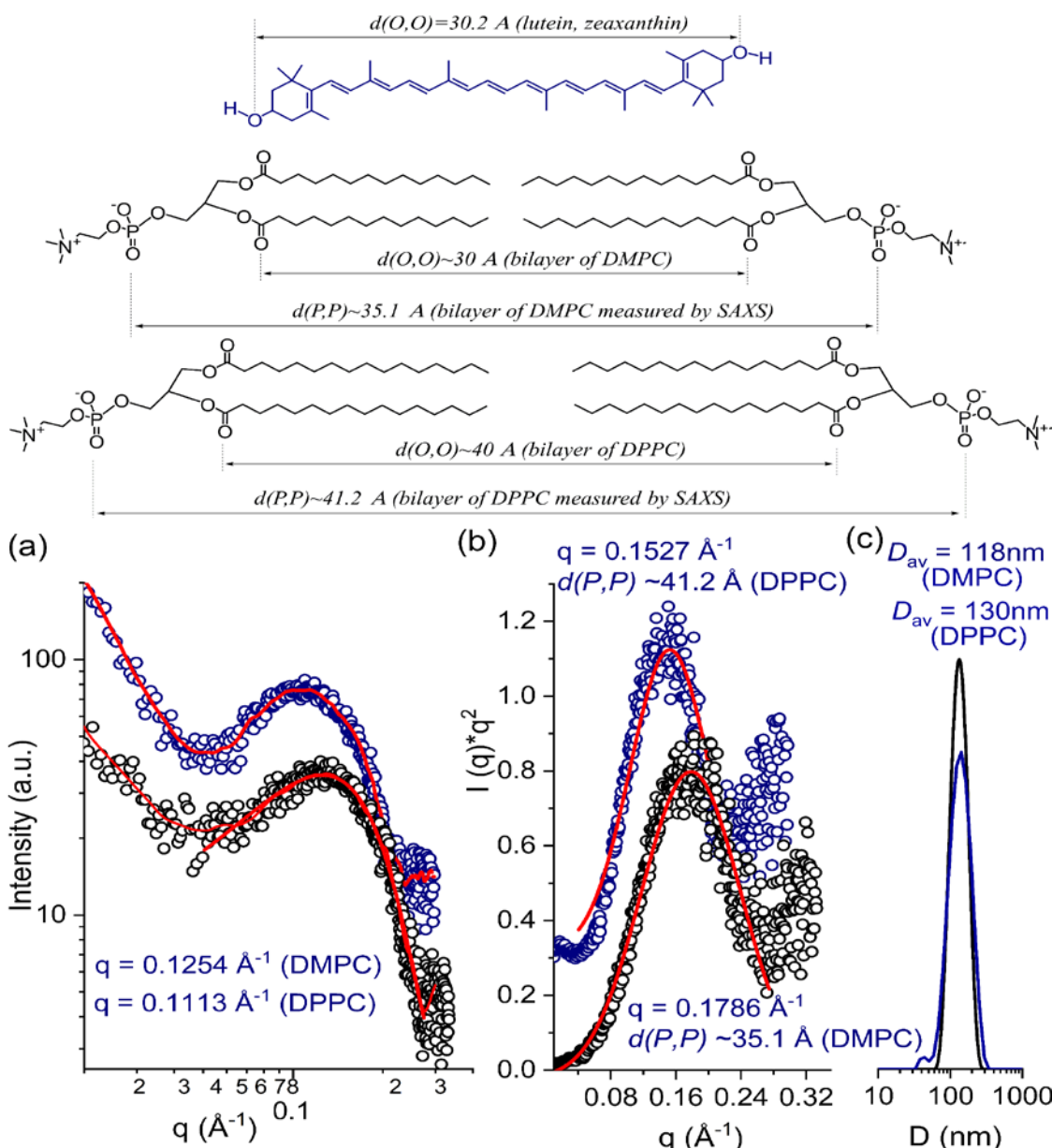


Figure 1. Top: Intramolecular dimensions of carotenoids and DMPC/DPPC bilayer as calculated by molecular mechanics [42,47]. The length of the carotenoid (lutein or zeaxanthin) corresponds to the length of the lipophilic segment of the DMPC phospholipid (double the average distance between the carbonyl group and the methyl group of the DMPC), and does not match the length of the lipophilic segment of the DPPC. Bottom: (a) SAXS data of DMPC-zeaxanthin (black) and DPPC-zeaxanthin (blue) LUVs; (b) Kratky plot from SAXS data, supporting the formation of unilamellar LUVs; and (c) Size distribution and the average diameter of DMPC-zeaxanthin (black) and DPPC-zeaxanthin (blue) LUVs measured by DLS (Figure S1).

3.2. Palmitoylation of Mouse BCO2 (mBCO2) in the Presence of Xanthophylls

We previously established that mBCO2 in eukaryotic HEK293F cells is palmitoylated. We discovered that in the presence of the mBCO2 substrate β -carotene mBCO2 loses palmitoylation [34]. Knowing that BCO2 cleaves xanthophylls [17,48,49] we decided to run palmitoylation assays to study the palmitoylation status of mBCO2 in the presence of xanthophylls. We first tried to deliver xanthophylls with the detergent Tween 40 [50]. We found that a higher concentration of Tween 40 (0.1%) led to HEK293F cell apoptosis as was previously described for HepG2 cells [51], while a lower concentration (0.01%) eluted mBCO2 from membranes during the Acyl-RAC assay even without hydroxylamine treatment (data not shown). Therefore, we established a new method to

deliver xanthophylls without detergents using unilamellar LUVs as described above. The content of xanthophylls in the HEK293F cells after 5 h of treatment was similar to a Tween 40 delivery system in ARPE-19 cells (1–2%) (Figure S2) [52]. Subsequently, we used the acyl-RAC method as described previously. The membrane fraction of HEK293F cells expressing mBCO2 was subjected to treatment with hydroxylamine (+HAM) and an equal portion of the fraction was treated with 250 mM NaCl (−HAM) which served as control. In the absence of substrates, mBCO2 protein showed an intense protein band in the HAM-treated sample (Figure 2A–D untreated panels, full Western blots are presented in Figure S3), while there was no protein band in the control NaCl-treated sample, indicating S-palmitoylation of BCO2 protein. In contrast, when cells were pre-treated with 0.15 μ M lutein and 0.06 μ M in DMPC/DMPS micelles, no protein band was detected in the HAM-treated sample (Figures 2A,B and S3A,D, lutein panel). Similar results were obtained with DPPC/DPPS-encapsulated zeaxanthin (0.45 μ M) (Figures 2C and S3B) and DMPC/DMPS-encapsulated violaxanthin (0.6 μ M) (Figures 2D and S3C).

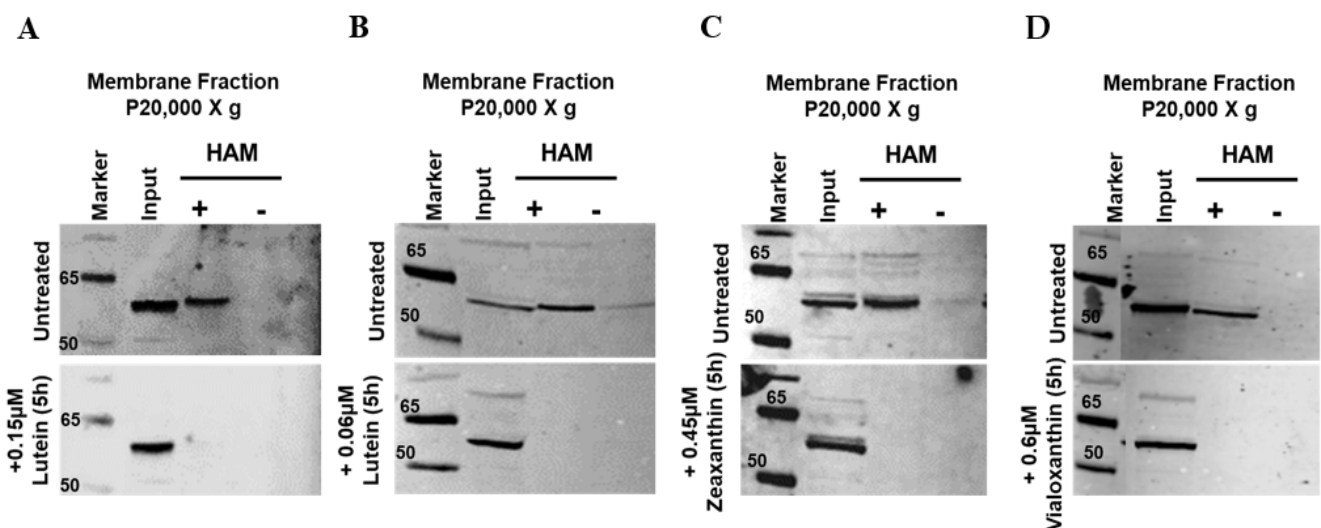


Figure 2. mBCO2 loses its palmitoylation in the presence of substrate. The palmitoylation status of mBCO2 protein was analyzed by Acyl-RAC assay in the presence of different substrates: (A) 0.15 μ M lutein; (B) 0.06 μ M lutein; (C) 0.45 μ M zeaxanthin; and (D) 0.6 μ M violaxanthin. Equal amounts (~50 μ g) of the total (indicated as “input”) and eluted protein from control (indicated as “−”) and hydroxylamine (HAM)-treated (indicated as “+”) were subjected to SDS-PAGE and immunoblotting. Western blot results are representative of three independent experiments as shown in the Supplementary figures.

3.3. Sub-Cellular Localization of mBCO2 with and without Xanthophylls. Shuttling the Enzyme to the Nucleus

Next, we examined BCO2 localization by immunofluorescence microscopy using mBCO2 transfected COS7 cells with various organelar markers (for mitochondria, peroxisomes, endoplasmic reticulum (ER), and Golgi). We confirmed that V5 tag antibodies recognize specifically mBCO2-V5 protein in transfected HEK293F cells (Figure S4). For nuclear labeling, we used DAPI nuclear stain. Immunofluorescence results as shown in Figure 3A (upper left panel) revealed the extensive mitochondrial colocalization with both COXIV and heat-shock protein 60 (HSP60) (Figure 3A, upper left panel). We did not observe any colocalization of mBCO2 with other organelles (Figures 3A, bottom left panel, and 4B) as indicated by their low correlation coefficient score compared with mitochondrial localization. Our data are in full agreement with previous results for human BCO2 [21,34]. However, upon addition of substrates to mBCO2 we observed that a fraction of mBCO2 colocalizes with the nuclear DAPI stain and the colocalization with mitochondrial markers is significantly decreased (Figure 3A, top right panel, C). The percent of colocalization with nuclear marker is higher when cells

are treated with lutein and violaxanthin (Figure 4A–C) than with zeaxanthin (Figure 5A–C).

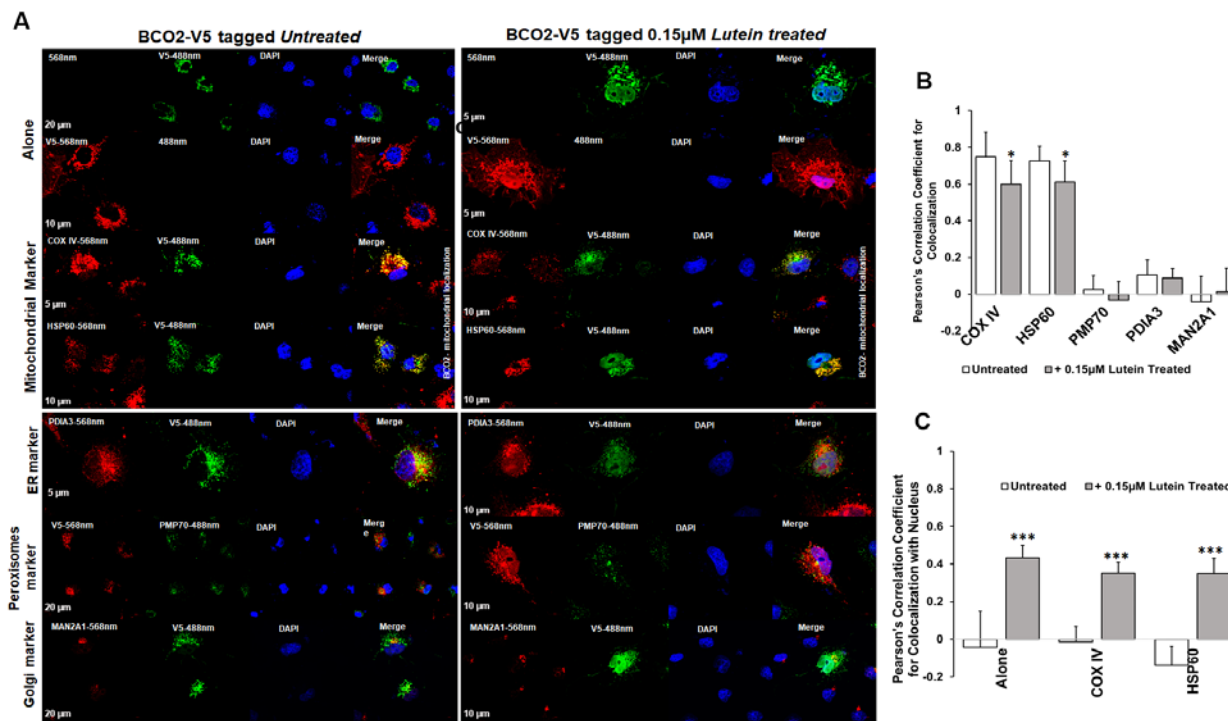


Figure 3. Characterization of subcellular localization of mBCO2 treated with lutein. (A) COS7 cells expressing mBCO2 protein treated with 0.15 μ M lutein for 5 h were immunoassayed using antibodies against V5 tag and different organelle marker proteins as indicated in the Materials and Methods section. Pearson's correlation coefficient for colocalization of V5-tagged mBCO2 protein with different organellar marker proteins (B) and with nucleus (C); * $p \leq 0.05$; *** $p \leq 0.0005$.

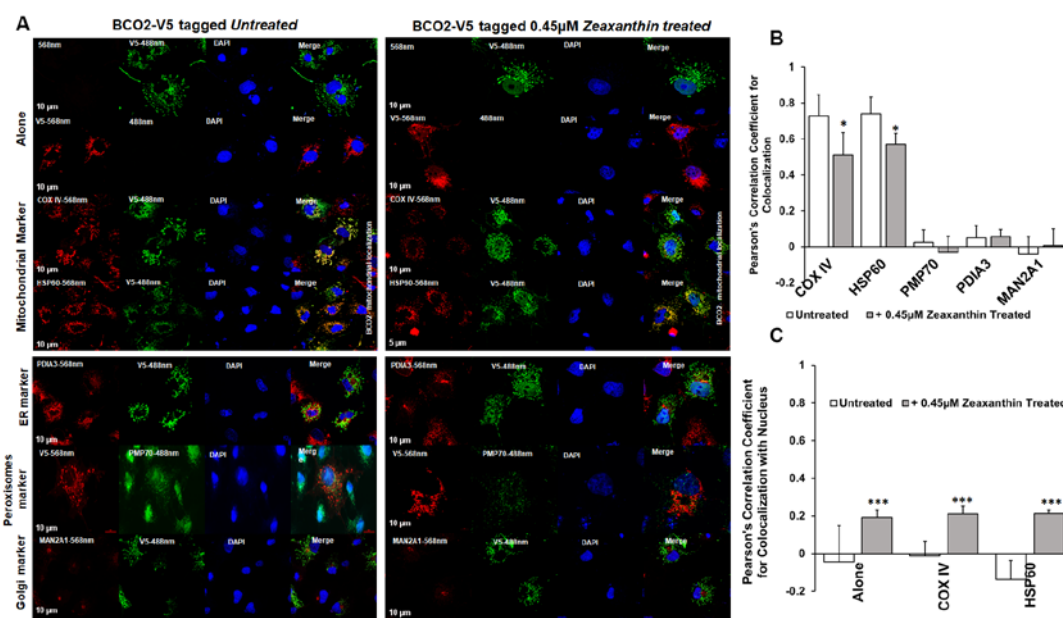


Figure 4. Characterization of subcellular localization of mBCO2 treated with zeaxanthin. (A) COS7 cells expressing V5-tagged mouse BCO2 protein treated with 0.45 μ M zeaxanthin for 5 h were immunoassayed using antibodies against V5 tag and different organelle marker proteins as indicated in the Materials and Methods section. Pearson's correlation coefficients were calculated for colocalization of V5-tagged mBCO2 protein with different organelle marker proteins (B) and with nucleus (C); * $p \leq 0.05$; *** $p \leq 0.0005$.

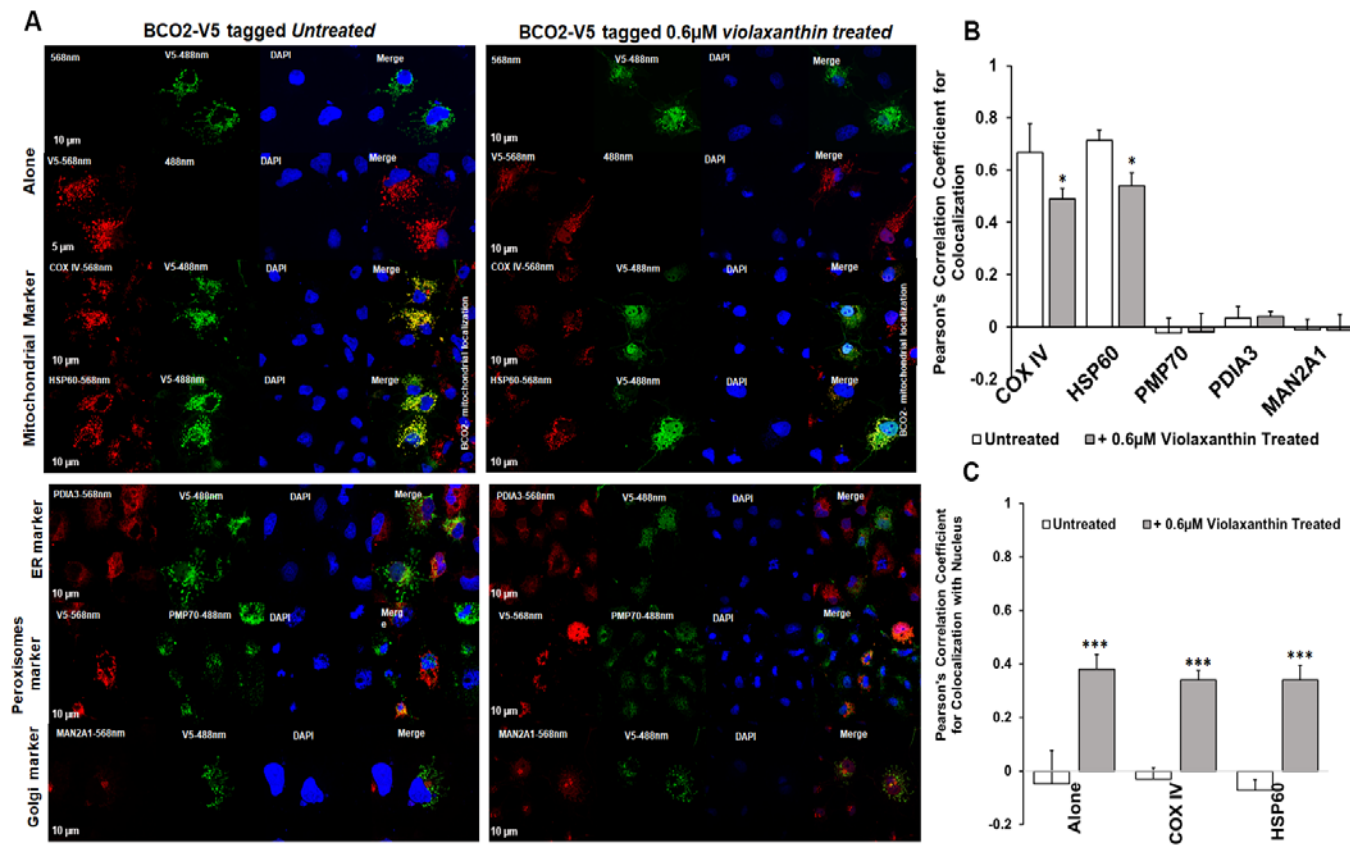


Figure 5. Characterization of subcellular localization of mBCO2 treated with violaxanthin. (A) COS7 cells expressing mBCO2 protein treated with 0.6 μ M violaxanthin for 5 h were immunoassayed using antibodies against V5 tag and different organelle marker proteins as indicated in the Materials and Methods section. Pearson's correlation coefficients were calculated for colocalization of V5-tagged mBCO2 protein with different organelar marker proteins (B) and with nucleus (C); * $p \leq 0.05$; *** $p \leq 0.0005$.

When we performed the experiment using a lower concentration of lutein (0.06 μ M) we observed that the percent colocalization of BCO2 in the nucleus decreased in a lutein concentration-dependent manner (Figure 6A–C). We have previously observed mBCO2 colocalization with the nuclear DAPI stain when cells were treated with β -carotene [34]. It correlates with our observation from the acyl-RAC assay that residual mBCO2 palmitoylation is seen in some samples in the presence of zeaxanthin, violaxanthin and a low concentration of lutein (Figure S3).

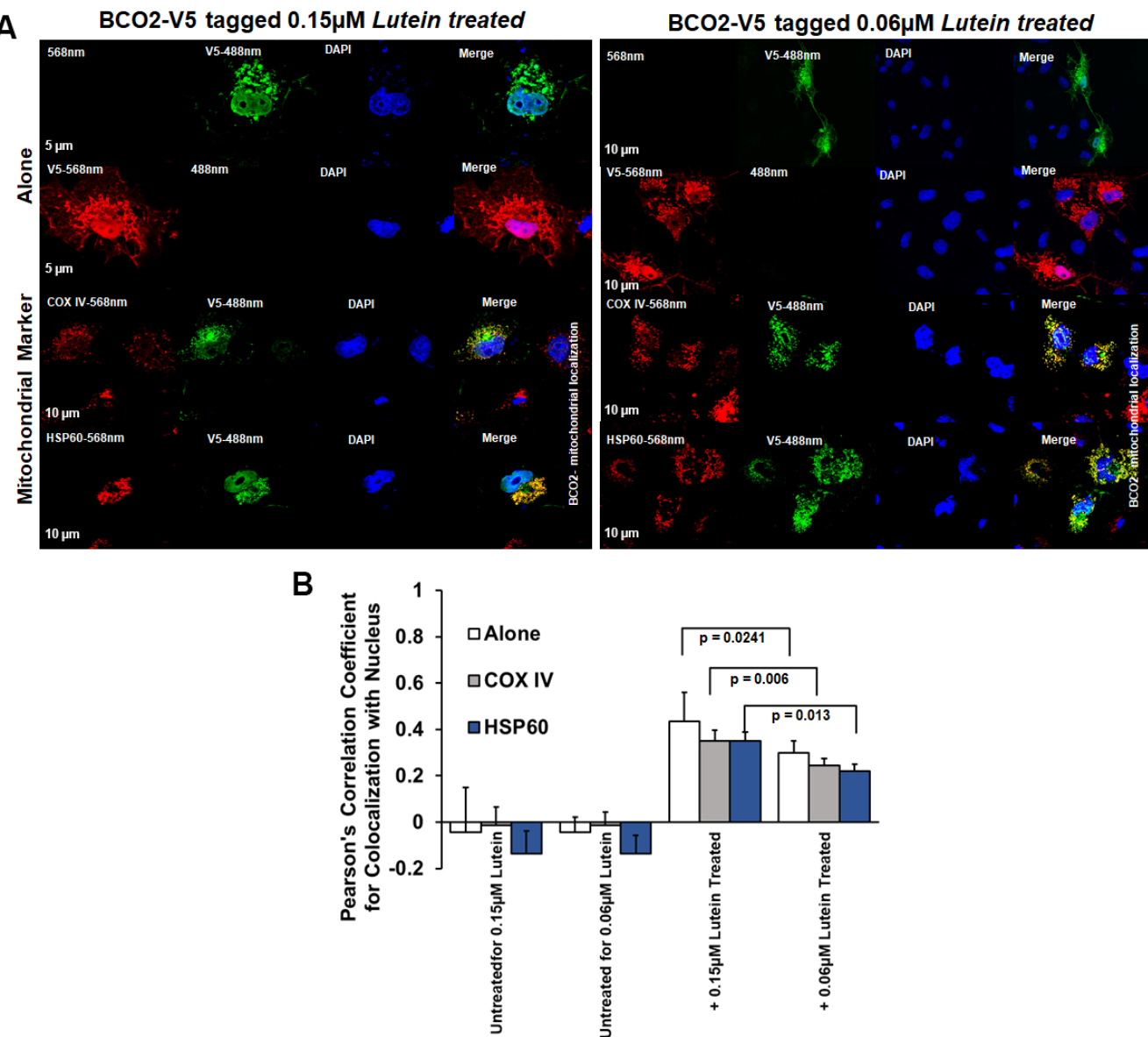


Figure 6. (A) Cellular Localization of V5-tagged mouse BCO2 with and without lutein: mBCO2 with and without 0.15 μ M lutein; (left panel) mBCO2 with and without 0.06 μ M lutein; (right panel). Pearson's correlation coefficients were calculated for colocalization of V5-tagged mBCO2 protein with nucleus (B).

3.4. Modeling of Xanthophyll Docking in Mouse BCO2

To understand these findings, we performed modeling of substrate (lutein, zeaxanthin and violaxanthin) docking in mBCO2. The Swiss-Model random coil model of the bovine RPE65 4F30 crystal with the helical -PDPCK- containing loop modeled in (using I-TASSER as described in Methods) was used as a basis to model mBCO2. We observed the highest binding energy to the Swiss-Model model of mBCO2 protein with lutein and the lowest with zeaxanthin. However, zeaxanthin binding energy significantly increased in Model1 (clash-free I-TASSER model which corrected the catalytic H and E residues orientation from the Swiss-Model model) docking simulation, while lutein and violaxanthin binding energy did not change (Table 1). Additionally, zeaxanthin did not line up well in the mBCO2 active site and curled up in both of the models (Figure 7A,B).

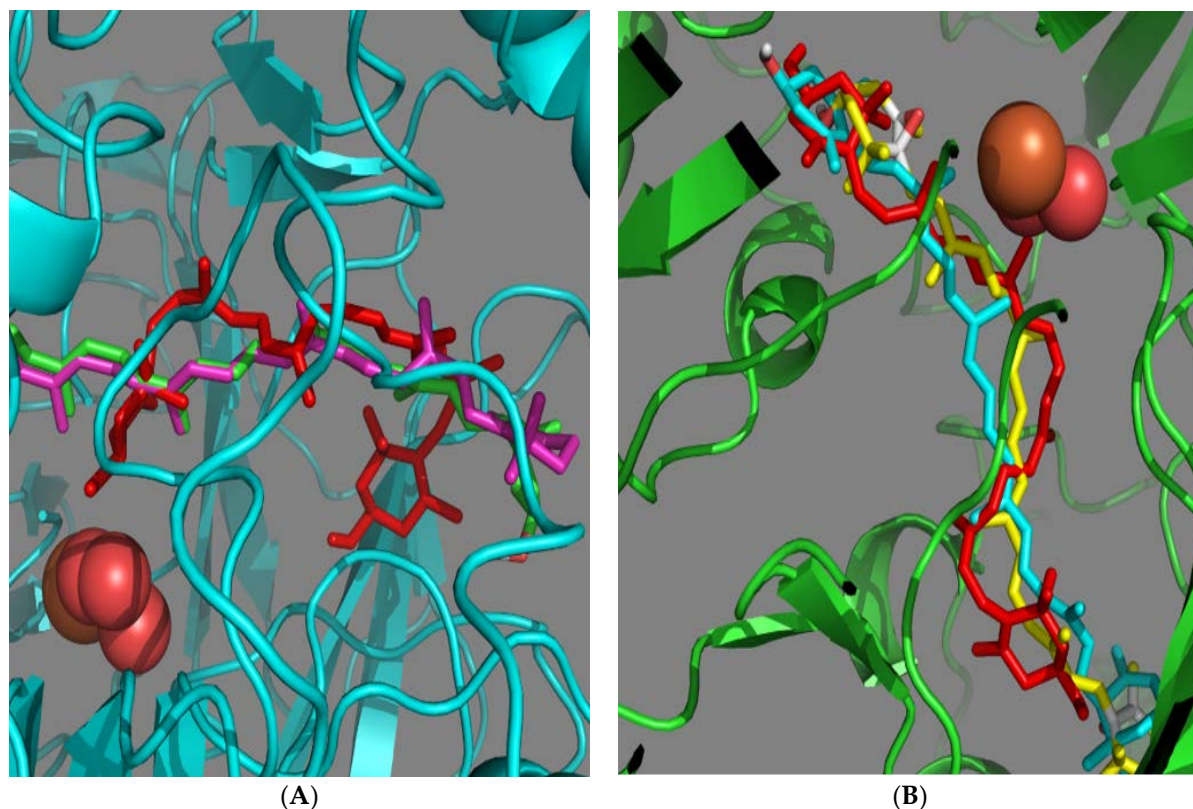


Figure 7. Visualization of carotenoid docking (A) on the mBCO2 protein I-TASSER model (lutein in green and β -carotene in purple, zeaxanthin in red and protein in cyan) and (B) on the mBCO2 protein Swiss-Model model (violaxanthin in yellow, lutein in cyan, zeaxanthin in red and protein in green).

Table 1. AutoDock Vina modeling of the affinity of carotenoids to mBCO2. The lowest (best) docking energy is used.

Carotenoid	SwissPro Model	I-TASSER Model1
violaxanthin	-11.0	-10.8
zeaxanthin	-11.8	-10.1
lutein	-10.5	-10.4
β -carotene	-11.8	-10.6

4. Discussion

Here we show that xanthophylls affect the palmitoylation status of mBCO2 and direct translocation of the enzyme to the nucleus where xanthophylls could modulate gene expression and exert antioxidant properties through activation of cellular oxidative stress response genes. To accomplish this, we developed a new unique non-disruptive way for membranes to deliver xanthophylls to cells. Thus, we produced LUVs with xanthophylls by using limonene to assist solubilization of the xanthophyll in bilayers made of phospholipids of the appropriate size. Our findings expand our previous findings regarding substrate-induced depalmitoylation and organellar relocalization of mBCO2 [34] and suggest a common effect of carotenoids on this enzyme.

The catalytic activity of mBCO2 towards certain oxidative metabolites of zeaxanthin was recently documented [17]. There are numerous other xanthophylls in the human diet. For example, violaxanthin is a diepoxy derivative of zeaxanthin and accumulates in a significant amount in human ovaries [53]. However, it was not known if it is a substrate and if mBCO2 could cleave it. Our results suggest that it does. It will be useful to better understand substrate structural requirements for mBCO2 function in cells.

Xanthophylls are well known for their antioxidant protective properties which may play a role in delaying chronic diseases. Despite this, it is still far from clear how xanthophylls exert the full extent of their antioxidant properties [54]. A widely proposed pathway is that they dissipate excess energy from potentially harmful oxidants, such as excited triplet states of singlet oxygen, by virtue of their extended conjugated bond systems and thereby protect membranes from oxidant stress [11]. Recently, however, a body of literature has begun to accumulate, pointing to direct regulation of gene expression by xanthophylls [50,55]. This would be analogous to the role of β -carotene metabolites in transcriptional regulation: β -apocarotenoids have been recently found to function as transcriptional regulators, specifically as nuclear receptor antagonists, which inhibit retinoic acid activities [56–59]. In this regard, lutein has been shown to activate Nrf2, an emerging regulator of cellular resistance to oxidants, and to affect Nrf2 pathway genes in retinal cells [50,60]. It has been demonstrated that lutein effectively protects ARPE-19 from damage generated by hyperglycemia by activating Nrf2 through its regulators, suggesting a preventive role of lutein against diabetic retinopathy [60]. How lutein (and other carotenoids/carotenoid metabolites) might enter the nucleus occurs is currently unknown.

In this respect, we previously described that presence of β -carotene changes the palmitoylation status of mBCO2 and that we can see residual colocalization with the nucleus [34]. Thus, our results with lutein, zeaxanthin and violaxanthin extend these prior findings by demonstrating that, generally, mBCO2 is palmitoylated in the absence of substrates and that it loses palmitoylation when substrates are present in the cells. Therefore, it prompts us to propose that loss of palmitoylation upon substrate-treatment somehow influences the BCO2-mitochondrial localization and promotes the shuttling of BCO2 to the nucleus. The mechanism of substrate bound-BCO2 shuttling to the nucleus is still unclear and needs to be investigated in further detail to explore the unclear function of BCO2 in the nucleus. Differences in binding of substrates to mBCO2 as demonstrated in our molecular docking experiments could define differences in nucleus shuttling and antioxidant effect of the various xanthophylls. Additionally, it is important to further study if mBCO2 could work as a transporter of xanthophylls and their metabolites to the nucleus (in addition to β -carotene and its metabolites), and to elucidate the potential mode of action of xanthophylls and their enzymatic metabolites on gene expression in relation to an oxidative stress response, in addition to their quenching properties.

Supplementary Materials: The following are available online at www.mdpi.com/2076-3921/10/3/413/s1, Figure S1: DLS data for LUVs with xanthophylls; Figure S2: Detection of mouse BCO2 palmitoylation by acyl-RAC assays. Raw Western blots; Figure S3: mBCO2 protein expression in the COS7 cells transfected with V5-tagged mBCO2. COS7 cells expressing mBCO2 protein treated with different substrates for 5h were grown on poly L-lysine coated coverslips and subjected to immunolocalization studies using confocal microscopy. For immunoblotting, post-nuclear supernatant was separated by SDS-PAGE. The presence of V5-tagged mBCO2 was probed by immunoblotting with rabbit polyclonal anti-mouse BCO2 (green) and mouse monoclonal anti-V5 (red) antibodies.

Author Contributions: Conceptualization, E.P. (Eugenia Poliakov); Methodology, S.U., E.P. (Eugenia Poliakov), S.A.D., W.Z., E.P. (Eugene Pinkhassik); formal analysis, S.U., S.A.D., E.P. (Eugenia Poliakov); resources, T.M.R., E.P. (Eugene Pinkhassik); data curation, modeling, docking S.G.; writing—original draft preparation, E.P. (Eugene Pinkhassik), S.A.D., S.U.; writing—review and editing, E.P. (Eugenia Poliakov), E.P. (Eugene Pinkhassik), S.A.D., and T.M.R. All authors have read and agreed to the published version of the manuscript.

Funding: This research was funded by the Intramural Research Program of the National Eye Institute, NIH (T.M. Redmond) and by the National Science Foundation (CHE-1709921; E. Pinkhassik).

Institutional Review Board Statement: Not applicable.

Data Availability Statement: The data presented in this study are available in this article and Supplementary material here.

Acknowledgments: Access to vSANS and NSE instruments was provided by the Center for High-Resolution Neutron Scattering, a partnership between the National Institute of Standards and Technology and the National Science Foundation under Agreement No. DMR-2010792. We acknowledge the support of the National Institute of Standards and Technology, U.S. Department of Commerce, in providing the neutron research facilities used in this work.

Conflicts of Interest: The authors declare no conflict of interest.

References

1. Bernstein, P.S.; Li, B.; Vachali, P.P.; Gorusupudi, A.; Shyam, R.; Henriksen, B.S.; Nolan, J.M. Lutein, zeaxanthin, and meso-zeaxanthin: The basic and clinical science underlying carotenoid-based nutritional interventions against ocular disease. *Prog. Retin. Eye Res.* **2016**, *50*, 34–66, doi:10.1016/j.preteyeres.2015.10.003.
2. Nolan, J.M.; Mulcahy, R.; Power, R.; Moran, R.; Howard, A.N. Nutritional Intervention to Prevent Alzheimer’s Disease: Potential Benefits of Xanthophyll Carotenoids and Omega-3 Fatty Acids Combined. *J. Alzheimer’s Dis.* **2018**, *64*, 367–378, doi:10.3233/jad-180160.
3. Bone, A.R.; Landrum, J.T.; Fernandez, L.; Tarsis, S.L. Analysis of the macular pigment by HPLC: Retinal distribution and age study. *Investig. Ophthalmol. Vis. Sci.* **1988**, *29*, 843–849.
4. Johnson, E.J.; Vishwanathan, R.; Johnson, M.A.; Hausman, D.B.; Davey, A.; Scott, T.M.; Green, R.C.; Miller, L.S.; Gearing, M.; Woodard, J.; et al. Relationship between Serum and Brain Carotenoids, alpha-Tocopherol, and Retinol Concentrations and Cognitive Performance in the Oldest Old from the Georgia Centenarian Study. *J. Aging Res.* **2013**, *2013*, 951786.
5. Rapp, L.M.; Maple, S.S.; Choi, J.H. Lutein and zeaxanthin concentrations in rod outer segment membranes from perifoveal and peripheral human retina. *Investig. Ophthalmol. Vis. Sci.* **2000**, *41*, 1200–1209.
6. Widomska, J.; Subczynski, W.K. Mechanisms enhancing the protective functions of macular xanthophylls in the retina during oxidative stress. *Exp. Eye Res.* **2019**, *178*, 238–246, doi:10.1016/j.exer.2018.06.012.
7. Grudzinski, W.; Nierzwicki, L.; Welc, R.; Reszczynska, E.; Luchowski, R.; Czub, J.; Gruszecki, W.I. Localization and Orientation of Xanthophylls in a Lipid Bilayer. *Sci. Rep.* **2017**, *7*, 1–10, doi:10.1038/s41598-017-10183-7.
8. Gruszecki, W.I.; Strzałka, K. Carotenoids as modulators of lipid membrane physical properties. *Biochim. Biophys. Acta BBA Mol. Basis Dis.* **2005**, *1740*, 108–115, doi:10.1016/j.bbadiis.2004.11.015.
9. Widomska, J.; Zareba, M.; Subczynski, W.K. Can Xanthophyll-Membrane Interactions Explain Their Selective Presence in the Retina and Brain? *Foods* **2016**, *5*, 7, doi:10.3390/foods5010007.
10. Delmelle, M. An Investigation of Retinal as a Source of Singlet Oxygen. *Photochem. Photobiol.* **1978**, *27*, 731–734, doi:10.1111/j.1751-1097.1978.tb07671.x.
11. Kim, S.R.; Nakanishi, K.; Itagaki, Y.; Sparrow, J.R. Photooxidation of A2-PE, a photoreceptor outer segment fluorophore, and protection by lutein and zeaxanthin. *Exp. Eye Res.* **2006**, *82*, 828–839.
12. Mortensen, A.; Skibsted, L.H. Free radical transients in photobleaching of xanthophylls and carotenes. *Free Radic. Res.* **1997**, *26*, 549–563, doi:10.3109/10715769709097826.
13. Adams, D.B.; Pozo, L.M.; Stewart, J.J.; Adams, W.W., 3rd. Zeaxanthin and Lutein: Photoprotectors, Anti-Inflammatories, and Brain Food. *Molecules* **2020**, *25*, 3607.
14. Connor, W.E.; Duell, P.B.; Kean, R.; Wang, Y. The Prime Role of HDL to Transport Lutein into the Retina: Evidence from HDL-Deficient WHAM Chicks Having a Mutant ABCA1 Transporter. *Investig. Ophthalmology Vis. Sci.* **2007**, *48*, 4226–4231, doi:10.1167/iovs.06-1275.
15. Loane, E.; Nolan, J.M.; Donovan, O.O.; Bhosale, P.; Bernstein, P.S.; Beatty, S. Transport and Retinal Capture of Lutein and Zeaxanthin with Reference to Age-related Macular Degeneration. *Surv. Ophthalmol.* **2008**, *53*, 68–81, doi:10.1016/j.survophthal.2007.10.008.
16. Li, B.; Vachali, P.; Frederick, J.M.; Bernstein, P.S. Identification of StARD3 as a Lutein-Binding Protein in the Macula of the Primate Retina. *Biochemistry* **2011**, *50*, 2541–2549, doi:10.1021/bi101906y.
17. Thomas, L.D.; Bandara, S.; Parmar, V.M.; Srinivasagan, R.; Khadka, N.; Golczak, M.; Kiser, P.D.; von Lintig, J. The human mitochondrial enzyme BCO2 exhibits catalytic activity toward carotenoids and apocarotenoids. *J. Biol. Chem.* **2020**, *295*, 15553–15565, doi:10.1074/jbc.ra120.015515.
18. Kiefer, C.; Hessel, S.; Lampert, J.M.; Vogt, K.; Lederer, M.O.; Breithaupt, D.E.; Von Lintig, J. Identification and Characterization of a Mammalian Enzyme Catalyzing the Asymmetric Oxidative Cleavage of Provitamin A. *J. Biol. Chem.* **2001**, *276*, 14110–14116, doi:10.1074/jbc.m011510200.
19. Amengual, J.; Lobo, G.P.; Golczak, M.; Li, H.N.M.; Klimova, T.; Hoppel, C.L.; Wyss, A.; Palczewski, K.; Von Lintig, J. A mitochondrial enzyme degrades carotenoids and protects against oxidative stress. *FASEB J.* **2010**, *25*, 948–959, doi:10.1096/fj.10-173906.
20. Lobo, G.P.; Isken, A.; Hoff, S.; Babino, D.; Von Lintig, J. BCDO2 acts as a carotenoid scavenger and gatekeeper for the mitochondrial apoptotic pathway. *Development* **2012**, *139*, 2966–2977, doi:10.1242/dev.079632.

21. Palczewski, G.; Amengual, J.; Hoppel, C.L.; Von Lintig, J. Evidence for compartmentalization of mammalian carotenoid metabolism. *FASEB J.* **2014**, *28*, 4457–4469, doi:10.1096/fj.14-252411.

22. Lindqvist, A.; He, Y.G.; Andersson, S. Cell type-specific expression of beta-carotene 9',10'-monooxygenase in human tissues. *J. Histochem. Cytochem.* **2005**, *53*, 1403–1412.

23. Wu, L.; Guo, X.; Wang, W.; Medeiros, D.M.; Clarke, S.L.; Lucas, E.A.; Smith, B.J.; Lin, D. Molecular aspects of beta, beta-carotene-9', 10'-oxygenase 2 in carotenoid metabolism and diseases. *Exp. Biol. Med.* **2016**, *241*, 1879–1887.

24. Väge, I.D.; A Boman, I. A nonsense mutation in the beta-carotene oxygenase 2 (BCO2) gene is tightly associated with accumulation of carotenoids in adipose tissue in sheep (*Ovis aries*). *BMC Genet.* **2010**, *11*, 10, doi:10.1186/1471-2156-11-10.

25. Berry, S.D.; Davis, S.R.; Beattie, E.M.; Thomas, N.L.; Burrett, A.K.; Ward, H.E.; Stanfield, A.M.; Biswas, M.; Udy, A.A.E.; Oxley, P.E.; et al. Mutation in bovine beta-carotene oxygenase 2 affects milk color. *Genetics* **2009**, *182*, 923–926.

26. Eriksson, J.; Larson, G.; Gunnarsson, U.; Bed'hom, B.; Boichard, T.M.; Stromstedt, L.; Wright, D.; Jungerius, A.; Vereijken, A.; Randi, E.; et al. Identification of the yellow skin gene reveals a hybrid origin of the domestic chicken. *PLoS Genet.* **2008**, *4*, doi:10.1371/journal.pgen.1000010.

27. Meyers, K.J.; Mares, J.A.; Igo, R.P.; Truitt, B.; Liu, Z.; Millen, A.E.; Klein, M.L.; Johnson, E.J.; Engelman, C.D.; Karki, C.K.; et al. Genetic Evidence for Role of Carotenoids in Age-Related Macular Degeneration in the Carotenoids in Age-Related Eye Disease Study (CAREDS). *Investig. Ophthalmology Vis. Sci.* **2014**, *55*, 587–599, doi:10.1167/iovs.13-13216.

28. Guo, X.; Wu, L.; Lyu, Y.; Chowanadisai, W.; Clarke, S.L.; Lucas, E.A.; Smith, B.J.; He, H.; Wang, W.; Medeiros, D.M.; et al. Ablation of be-ta,beta-carotene-9',10'-oxygenase 2 remodels the hypothalamic metabolome leading to metabolic disorders in mice. *J. Nutr. Biochem.* **2017**, *46*, 74–82.

29. Babino, D.; Palczewski, G.; Adhi, W.M.A.; Kiser, P.D.; Golczak, M.; von Lintig, J. Characterization of the Role of beta-Carotene 9,10-Dioxygenase in Macular Pigment Metabolism. *J. Biol. Chem.* **2015**, *290*, 24844–24857.

30. Li, B.; Vachali, P.P.; Gorusupudi, A.; Shen, Z.; Sharifzadeh, H.; Besch, B.M.; Nelson, K.; Horvath, M.M.; Frederick, J.M.; Baehr, W. Inactivity of human beta,beta-carotene-9',10'-dioxygenase (BCO2) underlies retinal accumulation of the human macular carotenoid pigment. *Proc. Natl. Acad. Sci. USA* **2014**, *111*, 10173–10178.

31. Poliakov, E.; Soucy, J.; Gentleman, S.; Rogozin, I.B.; Redmond, T.M. Phylogenetic analysis of the metazoan carotenoid oxygenase superfamily: A new ancestral gene assemblage of BCO-like (BCOL) proteins. *Sci. Rep.* **2017**, *7*, 3192, doi:10.1038/s41598-017-13521-x.

32. Dergunov, S.A.; Bowles, E.A.; Gordon, W.R.; Green, M.; Bierman, A.; Ellsworth, M.L.; Pinkhassik, E.; Sprague, R.S. Liposomal delivery of a phosphodiesterase 3 inhibitor rescues low oxygen-induced ATP release from erythrocytes of humans with type 2 diabetes. *Biochem. Biophys. Rep.* **2015**, *2*, 137–142, doi:10.1016/j.bbrep.2015.05.011.

33. Scott, H.L.; Skinkle, A.; Kelley, E.G.; Waxham, M.N.; Levental, I.; Heberle, F.A. On the Mechanism of Bilayer Separation by Extrusion, or Why Your LUVs Are Not Really Unilamellar. *Biophys. J.* **2019**, *117*, 1381–1386, doi:10.1016/j.bpj.2019.09.006.

34. Uppal, S.; Rogozin, I.B.; Redmond, T.; Poliakov, E. Palmitoylation of Metazoan Carotenoid Oxygenases. *Mol.* **2020**, *25*, 1942, doi:10.3390/molecules25081942.

35. Redmond, T.M.; Poliakov, E.; Yu, S.; Tsai, J.-Y.; Lu, Z.; Gentleman, S. Mutation of key residues of RPE65 abolishes its enzymatic role as isomerohydrolase in the visual cycle. *Proc. Natl. Acad. Sci. USA* **2005**, *102*, 13658–13663, doi:10.1073/pnas.0504167102.

36. Uppal, S.; Liu, T.; Poliakov, E.; Gentleman, S.; Redmond, T.M. The dual roles of RPE65 S-palmitoylation in membrane association and visual cycle function. *Sci. Rep.* **2019**, *9*, 5218, doi:10.1038/s41598-019-41501-w.

37. Waterhouse, A.; Bertoni, M.; Bienert, S.; Studer, G.; Tauriello, G.; Gumienny, R.; Heer, F.T.; de Beer, T.A.P.; Rempfer, C.; Bordoli, L.; et al. SWISS-MODEL: Homology modelling of protein structures and complexes. *Nucleic Acids Res.* **2018**, *46*, W296–W303, doi:10.1093/nar/gky427.

38. Roy, A.; Kucukural, A.; Zhang, Y. I-TASSER: A unified platform for automated protein structure and function prediction. *Nat. Protoc.* **2010**, *5*, 725–738, doi:10.1038/nprot.2010.5.

39. Roy, A.; Yang, J.; Zhang, Y. COFACTOR: An accurate comparative algorithm for structure-based protein function annotation. *Nucleic Acids Res.* **2012**, *40*, W471–W477, doi:10.1093/nar/gks372.

40. Zhang, Y. I-TASSER server for protein 3D structure prediction. *BMC Bioinform.* **2008**, *9*, 1–8, doi:10.1186/1471-2105-9-40.

41. Trott, O.; Olson, A.J. AutoDock Vina: Improving the speed and accuracy of docking with a new scoring function, efficient optimization, and multithreading. *J. Comput. Chem.* **2010**, *31*, 455–461.

42. Lazrak, T.; Milon, A.; Wolff, G.; Albrecht, A.M.; Miehe, M.; Ourisson, G.; Nakatani, Y. Comparison of the effects of inserted C40- and C50-terminally dihydroxylated carotenoids on the mechanical properties of various phospholipid vesicles. *Biochim. Biophys. Acta (BBA) Biomembr.* **1987**, *903*, 132–141, doi:10.1016/0005-2736(87)90163-5.

43. Nacke, C.; Schrader, J. Liposome based solubilisation of carotenoid substrates for enzymatic conversion in aqueous media. *J. Mol. Catal. B: Enzym.* **2011**, *71*, 133–138, doi:10.1016/j.molcatb.2011.04.009.

44. Socaci, C.; Jessel, R.; A Diehl, H. Carotenoid incorporation into microsomes: Yields, stability and membrane dynamics. *Spectrochim. Acta Part A: Mol. Biomol. Spectrosc.* **2000**, *56*, 2799–2809, doi:10.1016/s1386-1425(00)00375-9.

45. Strzałka, K.; Gruszecki, W.I. Effect of β -carotene on structural and dynamic properties of model phosphatidylcholine membranes. I. An EPR spin label study. *Biochimica et Biophysica Acta (BBA) Biomembranes* **1994**, *1194*, 138–142.

46. Chakraborty, S.; Doktorova, M.; Molugu, T.R.; Heberle, F.A.; Scott, H.L.; Dzikovski, B.; Nagao, M.; Stingaci, L.-R.; Standaert, R.F.; Barrera, F.N.; et al. How cholesterol stiffens unsaturated lipid membranes. *Proc. Natl. Acad. Sci. USA* **2020**, *117*, 21896–21905, doi:10.1073/pnas.2004807117.

47. Milon, A.; Ourisson, G.; Nakatani, Y. Organization of Carotenoid-Phospholipid Bilayer Systems. Incorporation of Zeaxanthin, Astaxanthin, and their C50 Homologues into Dimyristoylphosphatidylcholine Vesicles. *Helv. Chim. Acta* **1986**, *69*, 12–24, doi:10.1002/hlca.19860690104.

48. Dela Sena, C.; Sun, J.; Narayanasamy, S.; Riedl, K.M.; Yuan, Y.; Curley, R.W., Jr.; Schwartz, S.J.; Harrison, E.H. Substrate Specificity of Purified Recombinant Chicken beta-Carotene 9',10'-Oxygenase (BCO2). *J. Biol. Chem.* **2016**, *291*, 14609–14619.

49. Babino, D.; Golczak, M.; Kiser, P.D.; Wyss, A.; Palczewski, K.; von Lintig, J. The Biochemical Basis of Vitamin A3 Production in Ar-thropod Vision. *ACS Chem. Biol.* **2016**, *11*, 1049–1057.

50. Frede, K.; Ebert, F.; Kipp, A.P.; Schwerdtle, T.; Baldermann, S. Lutein Activates the Transcription Factor Nrf2 in Human Retinal Pigment Epithelial Cells. *J. Agric. Food Chem.* **2017**, *65*, 5944–5952, doi:10.1021/acs.jafc.7b01929.

51. Saadatmandi, B.C.; Rimbach, G.; Jungblut, A.; Frank, J. Comparison of tetrahydrofuran, fetal calf serum, and Tween 40 for the delivery of astaxanthin and canthaxanthin to HepG2 cells. *Cytotechnology* **2010**, *63*, 89–97, doi:10.1007/s10616-010-9324-7.

52. During, A.; Doraiswamy, S.; Harrison, E.H. Xanthophylls are preferentially taken up compared with beta-carotene by retinal cells via a SRBI-dependent mechanism. *J. Lipid Res.* **2008**, *49*, 1715–1724.

53. Semeniuk, C.E.; Wolczynski, S. Identification of carotenoids in ovarian tissue in women. *Oncol. Rep.* **2005**, *14*, 1385–1392, doi:10.3892/or.14.5.1385.

54. Perlman, M.J.A.; Millen, A.E.; Ficek, T.L.; Hankinson, S.E. The body of evidence to support a protective role for lutein and zeaxanthin in delaying chronic disease. Overview. *J. Nutr.* **2002**, *132*, 518S–524S.

55. Li, R.; Turner, S.D.; Brautigan, D.L. Xanthophylls lutein and zeaxanthin modify gene expression and induce synthesis of hyaluronan in keratinocyte model of human skin. *Biochem. Biophys. Rep.* **2015**, *4*, 52–58, doi:10.1016/j.bbrep.2015.08.012.

56. Eroglu, A.; Hruszkewycz, D.P.; Curley, R.W.; Harrison, E.H., Jr. The eccentric cleavage product of beta-carotene, be-ta-apo-13-carotenone, functions as an antagonist of RXRalpha. *Arch. Biochem. Biophys.* **2010**, *504*, 11–16.

57. Eroglu, A.; Hruszkewycz, D.P.; dela Sena, C.; Narayanasamy, S.; Riedl, K.M.; Kopec, R.E.; Schwartz, S.J.; Curley, R.W., Jr.; Harrison, E.H. Naturally occurring eccentric cleavage products of provitamin A beta-carotene function as antagonists of retinoic acid receptors. *J. Biol. Chem.* **2012**, *287*, 15886–15895.

58. Wang, C.X.; Jiang, H.; Yuen, J.J.; Lee, S.A.; Narayanasamy, S.; Curley, R.W., Jr.; Harrison, E.H.; Blaner, W.S. Actions of beta-apo-carotenoids in differentiating cells: Differential effects in P19 cells and 3T3-L1 adipocytes. *Arch. Biochem. Biophys.* **2015**, *572*, 2–10.

59. Ziouzenkova, O.; Orasanu, G.; Sukhova, G.; Lau, E.; Berger, J.P.; Tang, G.; Krinsky, N.I.; Dolnikowski, G.G.; Plutzky, J. Asymmetric cleavage of beta-carotene yields a transcriptional repressor of retinoid X receptor and peroxisome proliferator-activated receptor responses. *Mol. Endocrinol.* **2007**, *21*, 77–88.

60. Shivarudrappa, A.H.; Ponesakki, G. Lutein reverses hyperglycemia-mediated blockage of Nrf2 translocation by modulating the activation of intracellular protein kinases in retinal pigment epithelial (ARPE-19) cells. *J. Cell Commun. Signal.* **2019**, *14*, 207–221, doi:10.1007/s12079-019-00539-1.